Layer guided shear horizontally polarized acoustic plate modes

G. McHale[$], M. I. Newton and F. Martin

Department of Chemistry and Physics, The Nottingham Trent University
Clifton Lane, Nottingham NG11 8NS, UK

[$] Corresponding author: email: glen.mchale@ntu.ac.uk; Tel: +44 (0)115 8483383; Fax: +44 (0)115 9486636

Abstract

The theoretical basis describing Love waves propagating on a finite thickness substrate covered by a finite thickness solid layer having a lower shear acoustic speed is considered. A generalized dispersion equation is derived for shear horizontally polarized acoustic waves in this system. Two types of solutions to the dispersion equation, both satisfying stress free boundary conditions at the free surfaces, are shown to exist. The first type of solution has a displacement that decays with depth into the substrate whilst the second does not. Analytical approximations to the solutions for a thin solid guiding layer show that these solutions can be considered as generalizations of Love waves and resonant shear horizontally polarized acoustic plate modes (SH-APM), respectively. Numerical solutions to the dispersion equation are developed and the spectrum of modes for thick guiding layers is examined with particular reference to sensor applications. As expected, increasing the thickness of the guiding layer leads to multiple Love wave modes. However, each of these Love wave modes is found to possess a set of shear horizontally polarized acoustic plate modes. As the guiding layer thickness is increased the Love wave speed decreases until at approximately $v_l/4f$, where v_l is the shear acoustic speed of the layer and f is the frequency, a sharp transition occurs in the Love wave speed from a value close to the shear acoustic speed of the substrate, v_s, to one close to the shear acoustic speed of the layer, v_l. A similar pattern is observed for the layer guided SH-APM's with an increase in the guiding layer thickness resulting in a sharp transition in the speed of the SH-APM towards a value close to that of the next lower SH-APM. It is shown that the appearance of the second Love wave mode is a result of a continuation of the lowest SH-APM associated with the previous Love wave mode. A physical interpretation is developed for the Love waves on the finite substrate and for the layer guided SH-APM's and from this interpretation it is suggested that layer guided SH-APM sensors could provide significantly enhanced mass sensitivity.

Keywords Surface acoustic wave (SAW), Love wave, acoustic plate mode, SH-APM.

PACS Number 43.35

I. Introduction

Rayleigh surface acoustic waves (SAWs) have long been investigated for their use as sensors in gas phase applications[1]. However, the Rayleigh mode involves a surface normal component of displacement and in aqueous phase sensors this causes a compressional, or sound wave, to be generated in the liquid which results in large attenuation[2,3]. Flexural plate wave (FPW) devices also have a surface normal component of displacement, but the wave has a speed lower than the speed of sound in the liquid, which therefore prevents compressional wave generation and so allows them to be used as aqueous phase sensors[3]. FPW devices are relatively sophisticated to fabricate and, due to their thin substrates, are relatively fragile. For aqueous phase sensors the requirement for simple, robust devices has led to a focus on shear horizontally polarized acoustic waves which, in their idealised theory, do not suffer from significant compressional wave generation. The simplest of these devices is the quartz crystal microbalance (QCM) which operates at typical frequencies of 5-10 MHz. The term microbalance refers to the original Sauerbrey[4] view of the QCM as a sensor of the mass per unit area deposited on the crystal with a mass induced frequency shift, Δf, proportional to the product of the mass per unit area deposited on the crystal and the square of the operating frequency, i.e. $\Delta f/f = kf(\Delta m/A)$, where k is a constant. The frequency dependence of Rayleigh-SAW devices to the deposition of acoustically thin mass layers has the same form for the frequency and mass sensitivity. In liquid applications, the oscillation of the crystal induces a shear oscillation in the liquid which decays within a frequency dependent penetration depth of $\delta=(2\eta_f/\omega\rho_f)^{1/2}$, where η_f and ρ_f are the viscosity and density of the fluid and $\omega=2\pi f$ is the angular frequency. This viscous entrainment means the QCM only senses the mass of liquid within an interfacial layer and as a consequence the frequency shift is proportional to the viscosity-density product and a lower power of the frequency, i.e. $\Delta f/f = C(\eta_f\rho_f f)^{1/2}$, where C is a constant[5,6]. In liquid phase operation the quartz crystal also has a dissipation. The quartz crystal can also be used in electrochemical applications[7], biochemical applications[8] and with polymer layers[9], although in this latter case the response of the crystal is more complicated than when operated solely in a liquid[10-12].

In aqueous phase acoustic wave sensor applications, the trend has been for shear horizontal acoustic waves, to avoid compressional wave problems, and for higher frequencies, to gain higher sensitivity. Gas phase acoustic sensors have also sought higher sensitivity by increasing the operating frequency. However, QCMs use a thickness shear mode vibration and increasing frequency requires thinner, and hence more fragile, crystals. An alternative approach is to use surface acoustic waves generated by a set of interdigital transducers (IDTs)[13]. Thick piezoelectric substrates can then be used and the operating frequency is determined by the finger spacing of the IDTs which determines the wavelength. For the same lithographic resolution, a substrate with a higher speed for the wave results in a higher

operating frequency. Examples of surface acoustic wave device types with a dominant shear horizontal polarization include surface transverse waves[14] (STWs), leaky SAWs[15], surface skimming bulk waves[16] (SSBWs) and Love waves[17,18]. The Love wave configuration has been reported as having one of the highest mass sensitivities[19]. In aqueous phase sensing, one difficulty with these devices is the need to have an IDT on the same face of the substrate as the liquid. A combination of the practical advantages of a QCM and the SAW is provided by a sensor using shear horizontal acoustic plate modes (SH-APM's). These modes are also excited and detected by IDTs and do not have surface normal components of displacement, but they can be generated and detected by placing the IDTs on the opposite face of a thinned piezoelectric substrate[20,21]. However, the mass sensitivity of SH-APM devices is reported to be less than that of Love wave devices.

In the literature on sensors, the various types of acoustic waves are often regarded as completely separate. However, a consideration of the properties of Love wave and SH-APM devices as operated as sensors suggests much in common. In principle, a Love wave is a shear horizontally polarized acoustic wave that is localized to the surface of a semi-infinite half space and guided by a layer which has a shear acoustic speed less than that of the half space material[18]. In practice, the substrate is finite. The phase velocity of the Love wave is intermediate between that of the substrate and the layer and is determined by the layer thickness. In comparison, an acoustic plate mode occurs when a finite thickness substrate is excited at a natural resonant frequency of the substrate[22,23]. In practice, SH-APMs will also have a surface coating layer when operated as mass sensors and this mass layer is likely to possess a shear acoustic speed lower than that of the substrate. In theory, both the Love wave and the lowest order, n=0, SH-APM mode correspond to a plane wave. In Love wave theory, multiple modes can occur with the lowest order mode containing a node in the displacement at infinite depth into the substrate and an antinode at the free surface at the top of the guiding layer. In SH-APM theory, both the top face and lower face of the substrate are anti-nodes so that multiple modes occur with SH-APM modes corresponding to resonances of the plate matching a multiple of a half-wavelength condition. In a Love wave the phase speed is less than that of the shear acoustic speed of the substrate, whereas, in a SH-APM the phase speed is higher than that of the shear acoustic speed of the substrate. From a theoretical point of view, as operated, both Love waves and SH-APMs use finite substrates, both may have finite thickness mass layers with lower shear acoustic speeds than the substrate and both use a propagation parallel to the substrate with a surface transverse displacement. The primary difference appears to be that a Love wave requires a decaying displacement with depth into the substrate whilst a SH-APM uses a resonating solution. It should therefore be possible to describe both Love waves and mass coated SH-APMs using a single theoretical approach; that is the principal objective of this paper.

In this work, we develop a dispersion equation for waves with a surface transverse displacement propagating in the x_1-direction on a finite thickness substrate with faces oriented parallel to the x_2-x_3 plane and with one face coated a finite thickness solid overlayer. By imposing stress free boundary conditions at the lower substrate face and the upper face of the guiding layer, we show that Love waves and layer guided acoustic plate modes are two branches of solutions of the dispersion equation. The classification of the solutions as generalized Love waves and SH-APMs is justified by matching the analytical solutions for small guiding layer thickness to the known solutions for Love waves and SH-APM's; we therefore term the solutions generalized Love waves, although the SH-APM modes could equally well be termed layer guided SH-APMs. Further, numerical calculations of the solutions to the dispersion equation, show that each Love wave mode is accompanied by a set of acoustic plate modes. We also demonstrate that as the guiding layer thickness increases, the phase speed of the m=1 acoustic plate mode associated with a Love wave mode reduces until it transforms into the next higher order Love wave mode. Similarly, higher order SH-APM modes transform into lower order SH-APM modes associated with the next higher Love wave mode. The consequences of the derived phase speed dispersion curve for mass sensing applications are discussed. In addition, although we do not solve this system for contact with liquids, the theory does provide an insight into mass deposition from liquids and a theoretical basis for a generalization to liquid based sensors.

II. Theoretical Formulation

To simplify the problem, consider waves motion in an isotropic and non-piezoelectric material of density ρ and with Lamé constants λ and μ. The displacements, u_j, are then described by the equation of motion[18],

$$\rho \frac{\partial^2 u_j}{\partial t^2} = (\lambda + \mu) \frac{\partial S_{ii}}{\partial x_j} + \mu \underline{\nabla}^2 u_j \tag{1}$$

where the Einstein summation convention has been used and the strain tensor, S_{ij}, is defined as,

$$S_{ij} = \frac{1}{2}\left(\frac{\partial u_i}{\partial x_j} + \frac{\partial u_j}{\partial x_i} \right) \tag{2}$$

The boundary conditions on any solution require consideration of the stress tensor, T_{ij}, which can be written in the form,

$$T_{ij} = \lambda \delta_{ij} S_{kk} + 2\mu S_{ij} \tag{3}$$

In the combined Love wave and SH-APM problem, we consider a substrate of thickness, w, with a density ρ_s and Lamé constants λ_s and μ_s overlayed by a uniform mass layer of thickness, d, and with a density ρ_l and Lamé constants λ_l and μ_l. In analogy to Love wave theory, the uniform mass overlayer will also be

referred to as the guiding layer. The upper surface of the substrate is taken to be in the (x_1, x_2) plane and located at x_3=0 (Fig. 1). The solutions of the equation of motion are chosen to have a propagation along the x_1 axis with displacements in the x_2 direction of the sagittal plane (x_2, x_3). They must also satisfy the boundary conditions that both $\underline{u}$ and the T_{i3} component of the stress tensor are continuous at the interface between the substrate and layer and that the T_{i3} component of the stress tensor vanishes at the free surfaces of the substrate and layer at x_3=-w and x_3= d, respectively.

In order to preserve the notational similarity with the Love wave problem, a solution for the equation of motion is sought by using displacements in the layer, $\underline{u}_l$, and the substrate, $\underline{u}_s$, of

$$\underline{u}_l = (0,1,0)\left[A_l e^{-jT_l x_3} + B_l e^{jT_l x_3}\right] e^{j(\omega t - k_1 x_1)} \tag{4}$$

and

$$\underline{u}_s = (0,1,0)\left[C_s e^{T_s x_3} + D_s e^{-T_s x_3}\right] e^{j(\omega t - k_1 x_1)} \tag{5}$$

where ω is the angular frequency and the wave vector is $k_1=(\omega/v)^{1/2}$ where v is the phase speed of the solution. A_l, B_l, C_s and D_s are constants determined by the boundary conditions. A traditional Love wave solution occurs when the substrate thickness $w \rightarrow \infty$, the shear speed of the substrate, $v_s= (\mu_s/\rho_s)^{1/2}$, is greater than the shear speed of the layer, $v_l= (\mu_l/\rho_l)^{1/2}$, and the wave vector T_s is real, so that the solution, $\underline{u}_s$, decays with depth into the substrate. A traditional SH-APM solution occurs when $d \rightarrow 0$ and the wave vector T_s is purely imaginary, so that the solution, $\underline{u}_s$, may take on a standing wave (resonant) form. In the more general case under consideration here, both T_l and T_s may be complex rather than real. The use of the exponentials with a j factor in Eq. (4) and without a j factor in Eq. (5) is therefore purely to enable the similarity with the Love wave theory to be more readily noted.

Substituting Eq. (5) into the equation of motion describing the substrate, i.e. Eq. (1) with the substrate parameters, gives the equation for the wave vector T_s,

$$T_s^2 = \omega^2\left(\frac{1}{v^2} - \frac{1}{v_s^2}\right) \tag{6}$$

Similarly substituting Eq. (4) into the equation of motion describing the layer, gives

$$T_l^2 = \omega^2\left(\frac{1}{v_l^2} - \frac{1}{v^2}\right) \tag{7}$$

To completely specify the problem the boundary conditions are imposed and this defines the constants A_l, B_l, C_s and D_s in Eqs. (4) and (5). The first boundary condition is continuity of the displacement at the interface between the substrate and the layer at x_3=0 and this gives,

$$A_l + B_l = C_s + D_s \tag{8}$$

The remaining conditions all relate to the T_{i3} component of the stress tensor, which for this system using the form of the solutions in Eqs. (4) and (5) can be written as,

$$T_{i3} = \delta_{i2}\mu\left(\frac{\partial u_2}{\partial x_3}\right) \tag{9}$$

The second boundary condition, continuity of T_{i3} at the substrate-layer interface, gives,

$$-A_l + B_l = -j(C_s - D_s)\xi \tag{10}$$

where ξ has been defined as,

$$\xi = \frac{\mu_s T_s}{\mu_l T_l} \tag{11}$$

The remaining two boundary conditions are continuity of stress at the two free surfaces at x_3=d and x_3=-w, and these give the equations,

$$A_l \exp(-jT_l d) - B_l \exp(jT_l d) = 0 \tag{12}$$

and

$$C_s \exp(-T_s w) - B_s \exp(T_s w) = 0 \tag{13}$$

Solving the boundary conditions, Eqs (8), (10), (12) and (13), gives both a dispersion equation,

$$\tan(T_l d) = \xi \tanh(T_s w) \tag{14}$$

and the solutions for the displacements,

$$\underline{u}_l = (0,1,0)A\exp(-T_s w)\left[\cosh(T_s w)\cos(T_l x_3) + \xi \sinh(T_s w)\sin(T_l x_3)\right]e^{j(\omega t - k_1 x_1)} \tag{15}$$

and

$$\underline{u}_s = (0,1,0)A\exp(-T_s w)\cosh\left[T_s(x_3 + w)\right]e^{j(\omega t - k_1 x_1)} \tag{16}$$

where ξ is defined by Eq. (11) and A is a constant. Using the dispersion equation (Eq. (14)) the layer displacement may be re-written as,

$$\underline{u}_l = (0,1,0)A\exp(-T_s w)\cosh(T_s w)\left[\cos(T_l x_3) + \tan(T_l d)\sin(T_l x_3)\right]e^{j(\omega t - k_1 x_1)} \tag{17}$$

III. Structure of solutions

The dispersion equation (Eq. (14)) is highly non-linear, but can nonetheless be solved numerically and the phase speed obtained for the various possible modes for given substrate and layer depths with specific material properties (shear speeds, densities, etc). However, it is useful for matching the theory to Love wave and SH-APM theory to consider the perturbation solutions for finite thickness substrates covered by mass layers of small thickness. Before performing a perturbation expansion, it is instructive to consider the structure of the dispersion equation and how it relates to Love waves and SH-APM's and to multiple modes.

a) Love waves

When T_s is real and positive and the substrate thickness $w \to \infty$, the dispersion equation (Eq. (14)) reduces to the dispersion equation for the Love wave case,

$$\tan(T_l d) = \xi \tag{18}$$

When T_s is real and positive, but w is finite we have a solution with a substrate displacement that decays with depth and which can therefore be regarded as a Love wave solution on a finite substrate. This finite substrate Love wave case contains multiple Love wave modes due to the $\tan(T_l d)$ term[18]. At the start of each of these modes the conditions satisfied are,

$$\tan(T_l d) = 0 \tag{19}$$

and

$$\xi = \frac{\mu_s T_s}{\mu_l T_l} = 0 \tag{20}$$

so that the phase speed at the start of each mode is given from Eq. (6), using T_s=0, as v=v_s and the start of the multiple Love wave modes are given by $T_l d = n\pi$ where n=0, 1, 2, ... As the thickness, d, of the guiding layer increases, the phase speed decreases non-linearly from a value equal to the shear speed of the substrate towards the value of the shear speed of the layer, v_l. The existence of multiple modes means that we can consider a perturbation expansion about the start of each mode, rather than simply about a zero thickness mass layer. Essentially, the perturbation theory for higher Love wave modes starts at a finite guiding layer thickness and is a perturbation of the phase speed from the value of the substrate shear speed. A necessary part of the Love solution is that the phase speed is equal to or less than the phase speed

of the substrate. It is this condition that guarantees T_s real and an exponential decay of the displacement with depth into the substrate.

b) SH-APM's

The dispersion equation (Eq. (14)) reduces to the dispersion equation for the SH-APM case when T_s is purely imaginary, the substrate thickness w is finite and the mass overlayer vanishes ($d \to 0$). In this case, it is possible to write $T_s = jk_s$ with k_s real. The dispersion equation then requires either $\xi = 0$ or a solution of the equation,

$$\tan(k_s w) = 0 \tag{21}$$

The possible solutions of Eq (21) are the different resonating modes of the SH-APM and are,

$$k_s = \frac{m\pi}{w} \qquad m = 0, 1, 2, 3, \ldots \tag{22}$$

Substituting Eq (22) into Eq (6) gives the phase speed,

$$v_m = \frac{v_s}{\sqrt{1 - \left(\frac{m\pi v_s}{W\omega}\right)^2}} \tag{23}$$

where the subscript m has been added to the phase speed, v, to indicate its dependence on the mode number. Thus, the phase speeds of the SH-APM modes are either equal to or greater than the shear speed of the substrate. It is this condition that guarantees T_s imaginary and a standing wave resonance in the substrate.

c) Love waves and Layer Guided APM's

In the case that a SH-APM occurs (i.e. T_s is purely imaginary), but a finite thickness mass overlayer exists, there will be a set of solutions to Eq (14) for every value of d. Moreover, as the overlayer thickness increases, the phase speed associated with each of these modes will decrease. For this reason, the m=0 SH-APM mode used in sensing, should not be regarded as a SH-APM mode at all. The slightest mass loading will lower its phase speed to below that of the substrate so that the wavevector in the substrate will change from imaginary to real and it will therefore become the first Love wave mode.

Eq. (23) also shows that for any given frequency there is a maximum number of SH-APM modes, $m_{\max}$, since the phase speed, v_m, must be finite,

$$m_{\max} = \frac{W\omega}{\pi v_s} \tag{24}$$

In the solution of the full dispersion equation (Eq. (14)), the guiding layer thickness and the phase speed can be chosen to simultaneously satisfy both the Love wave condition $\tan(T_l d)=0$ and the SH-APM condition $\tan(k_s w)=0$. The thickness, d_{nm}, and the phase speed, v_m, at which modes satisfies these conditions can be regarded as the start of a mode; this definition of the start of a mode is then consistent with the traditional view of the start of a Love wave mode. The thickness at which a mode starts is then given from Eq. (19) and Eq. (23) as,

$$\frac{d_{nm}}{\lambda_l} = \frac{n}{2\sqrt{1-\left(\frac{v_l}{v_m}\right)^2}} = \frac{n}{2\sqrt{1-\left(\frac{v_l}{v_s}\right)^2\left[1-\left(\frac{m\lambda_s}{2w}\right)^2\right]}} \tag{25}$$

where n=0,1,2,3, …. labels the successive Love wave modes and m=1,2,3, … labels the acoustic plate modes associated with each Love wave mode. As the thickness of the guiding layer increases, the phase speed of each plate mode associated with a particular Love wave mode decreases until at some guiding layer thickness it attains the value of the next lower plate mode associated with the next higher order Love wave mode.

IV. Perturbation Solutions

In the previous section the structure of the solutions to the dispersion equation (Eq. (14)) has been discussed and the similarities with Love waves and SH-APM's has been illustrated. In addition, the effect on Love waves of a finite thickness substrate and on SH-APM's of a guiding layer has also been highlighted. In order to convincingly demonstrate that the theoretical formulation does encompass traditional Love waves and SH-APM's, perturbation theory is used in this section to obtain the limiting case of small mass loading whose results are known in the literature. Consider a perturbation, Δd, of the guiding layer thickness, d, from d=0 for the n=0 Love wave and associated SH-APM's. The phase speed of the unperturbed case of no guiding layer is known and given by Eq. (23) and this perturbation will result in a decrease in the phase speed of the mode. The perturbation $d=0 \rightarrow d=\Delta d$ will cause changes in the phase speed and the wavevectors and we can therefore write $T_l \,^{o}\!\rightarrow T_l \,^{o}\!+\Delta T_l$, $T_s \,^{o}\!\rightarrow T_s \,^{o}\!+\Delta T_s$ and $\xi^{o}\rightarrow\xi^{o}+\Delta\xi$ where the superscript zero indicates the values of the quantities when d=0. The dispersion equation (Eq. (14)) can then be written,

$$\tan(T_l^o \Delta d) \approx \frac{(\xi^o + \Delta\xi)\tanh(\Delta T_s w) + \Delta\xi \tanh(T_s^o w)}{1 + \tanh(T_s^o w)\tanh(\Delta T_s w)} \tag{26}$$

Further approximation depends on whether the mode being perturbed is a Love wave (ξ^o=0) or one of the associated m>0 SH-APM's ($\tanh(T_s^o w)$=0, but $\xi^o \neq 0$).

a) Love wave case

The n=0 Love wave case satisfies ξ^o=0 and this requires T_s^o=0 so that, from Eq. (6), v^o=v_s. Eq. (26) reduces to,

$$\tan(T_l^o \Delta d) \approx \Delta\xi \tanh(\Delta T_s w) \tag{27}$$

Considering the definition of ξ (Eq. (11)) the perturbation $\Delta\xi$ can be written in terms of the wavevectors and their perturbations,

$$\Delta\xi \approx \frac{\mu_s \Delta T_s}{\mu_l T_l^o} \tag{28}$$

The perturbation in T_s arises from the perturbation to the phase speed and is given from Eq. (6) as,

$$\Delta T_s \approx \frac{\omega}{v_s}\sqrt{\frac{-2\Delta v}{v_s}} \tag{29}$$

Eq (27) therefore becomes,

$$\tan(T_l^o \Delta d) \approx \frac{\mu_s \omega}{\mu_l v_s T_l^o}\sqrt{\frac{-2\Delta v}{v_s}} \tanh\left(\frac{\omega w}{v_s}\sqrt{\frac{-2\Delta v}{v_s}}\right) \tag{30}$$

where

$$T_l^o = \omega\sqrt{\frac{1}{v_l^2} - \frac{1}{v_s^2}} \tag{31}$$

The left-hand side of Eq (30) is similar in form to that used in acoustic load impedance models of quartz crystal microbalances[12]. In QCM models, the acoustic load, Z_L, on the crystal due to a thin mass layer is $Z_L = j(\mu_l/v_l)\tan(\omega \Delta d/v_l)$ and the periodicity in this causes shear wave resonances[10-12]. To first order in the mass layer thickness Eq. (30) becomes,

$$\Delta d \approx \frac{\mu_s v_s \sqrt{\frac{-2\Delta v}{v_s}}}{\mu_l \omega \left(\frac{v_s^2}{v_l^2} - 1 \right)} \tanh\left(\frac{\omega w}{v_s} \sqrt{\frac{-2\Delta v}{v_s}} \right) \tag{32}$$

The result in Eq. (32) gives the perturbation in the phase speed due to the presence of a small mass layer acting as a wave guide on a finite thickness substrate. The traditional Love wave assumes an infinitely thick substrate and this can be obtained by taking the limit $w \to \infty$, so that the tanh() term tends to unity. This gives,

$$\frac{\Delta v}{v_s} \approx -\frac{1}{2} \left[\frac{\mu_l \left(\frac{v_s^2}{v_l^2} - 1 \right) \omega \Delta d}{\mu_s v_s} \right]^2 \tag{33}$$

Thus, a thin mass layer acting as a Love wave guide on an infinite thickness substrate generates a fractional shift in the phase speed proportional to the square of the product of the frequency and mass thickness (or frequency and mass per unit area). In many practical situations the substrate phase velocity is much larger than the layer phase speed and Eq. (33) can be further simplified.

b) SH-APM with *m*=0

In this sub-section a perturbation expansion is used for the m=0 SH-APM and a result identical to that existing in the literature is obtained. It is then shown that this result is in error due to the perturbation being about a singular point which means that a perturbed m=0 SH-APM mode becomes a Love wave rather than remaining as a SH-APM. The zeroth order plate mode is given by a finite thickness substrate with $T_s = jk_s$ and $k_s w = 0$. This necessarily means it also satisfies the Love wave condition for the unperturbed system of $\xi^0 = 0$ and, from Eq. (6), the unperturbed phase speed is v_s. The perturbation expansion of the dispersion equation (Eq. (14)) follows the finite thickness substrate Love wave case and Eqs (30)-(32) are obtained. However, in the SH-APM case the substrate thickness remains finite and we expand the tanh() term on the right hand side of Eq. (30),

$$\frac{\Delta v}{v_s} \approx \frac{-\mu_l v_s}{2\mu_s w \omega} \sqrt{\frac{v_s^2}{v_l^2} - 1} \tan\left(\sqrt{\frac{v_s^2}{v_l^2} - 1} \frac{\omega \Delta d}{v_s} \right) \tag{34}$$

Again, Eq (30) has been used initially, rather than going directly to Eq. (33), in order to preserve the similarity in form to acoustic impedance models of QCM's. Expanding in small layer thickness gives,

$$\frac{\Delta v}{v_s} \approx \frac{-\mu_l}{2\mu_s}\left(\frac{v_s^2}{v_l^2}-1\right)\frac{\Delta d}{w} \tag{35}$$

which can be re-written using $v_s = (\mu_s/\rho_s)^{1/2}$ and $v_l = (\mu_l/\rho_l)^{1/2}$. In the approximation that $(v_s/v_l)^2 >> 1$, Eq. (35) reduces to,

$$\frac{\Delta v}{v_s} \approx \frac{-\rho_l \Delta d}{2\rho w_s} \tag{36}$$

which is precisely the result given by Martin *et al*[23] for the sensitivity of the SH-APM mode 0 to small mass perturbations. However, we argue that the above calculation is in fact in error due to the perturbation being singular. The problem arises because the predicted velocity shift is negative and this must reduce the phase speed to a value below that of the substrate. However, in this case Eq. (6) predicts that T_s^2 will be positive and so the assumption that $T_s = jk_s$ with k_s real can no longer be valid. In effect, when the phase speed of the m=0 SH-APM is perturbed by a mass layer of shear speed lower than the substrates, the solution necessarily converts into a Love wave.

c) SH-APM with m>0

The higher order SH-APM's associated with the Love wave do not suffer the same difficulty as the m=0 SH-APM. In this case, the unperturbed solution has $\tanh(T_s^o w)=0$ with $T_s^o = jk_s^o$ and k_s^o real, but with $\xi^o \neq 0$. Thus, the unperturbed phase speed v_m of the m^{th} mode is not equal to the shear speed of the substrate v_s and it is possible to perturb the phase speed without breaking the assumption that k_s is real and so retain a SH-APM mode. In the m>0 SH-APM case, Eq. (26) reduces to,

$$\tan(T_l^o \Delta d) \approx \xi^o \tanh(\Delta T_s w) \tag{37}$$

and Eq. (6) gives,

$$\Delta T_s \approx \frac{-\omega^2}{v_s}\frac{\Delta v}{v_m^3} \tag{38}$$

Thus, the equivalent of Eq. (30) is,

$$\tan(T_l^o \Delta d) \approx \frac{\mu_s \omega}{\mu_l v_m T_l^o} \sqrt{\frac{v_m^2}{v_s^2} - 1} \tan\left(\frac{\omega w}{v_m \sqrt{\frac{v_m^2}{v_s^2} - 1}} \left(\frac{-\Delta v}{v_m} \right) \right) \tag{39}$$

where T_l^o is given by

$$T_l^o = \omega \sqrt{\frac{1}{v_l^2} - \frac{1}{v_m^2}} \tag{40}$$

Significant differences between Eq. (30) describing Love waves and Eq. (39) describing SH-APM's include the replacement of the tanh( ) on the right-hand side by a tan( ) term, the replacement of the $(-2\Delta v/v_s)^{1/2}$ by $(-\Delta v/v_m)$ in the argument of the tan( ) and the lack of a pre-factor involving the perturbation to the phase speed. A further difference is the presence of a $(v_m^2/v_s^2-1)^{1/2}$ as a prefactor to the tan( ) and in the denominator of the argument of the tan( ). This factor is responsible for the difficulties with the m=0 SH-APM mode because when m=0 the unperturbed phase speed, v_m, is equal to the substrate phase speed, v_s, and the factor vanishes, thus giving a singularity in the argument of the tan( ) term. However, if this singularity is formally ignored and the tan( ) is expanded to first order, the factor from the argument cancels with the factor in the pre-factor and an apparent result for the perturbation to the phase speed can be obtained. We believe this formal perturbation result for the m=0 SH-APM mode is invalid and that, in fact, the mode becomes a Love wave with the perturbation to the phase speed described by Eq. (30).

For the m>0 SH-APM modes, Eq. (39) can be written to first order in Δd as,

$$\Delta d \approx \frac{\mu_s v_m \sqrt{\frac{v_m^2}{v_s^2} - 1}}{\mu_l \omega \left(\frac{v_m^2}{v_l^2} - 1 \right)} \tan\left(\frac{\omega w}{v_m \sqrt{\frac{v_m^2}{v_s^2} - 1}} \left(\frac{-\Delta v}{v_m} \right) \right) \tag{41}$$

and expanding to first order in Δv gives,

$$\frac{\Delta v}{v_m} \approx \frac{-\mu_l}{\mu_s} \left(\frac{v_m^2}{v_l^2} - 1 \right) \frac{\Delta d}{w} \tag{42}$$

which is a factor of two greater than Eq. (35). Eq. (23) can be used to evaluate the mode speed v_m from the substrate speed and thickness and the operating frequency. In the case that the unperturbed SH-APM modes are close in phase speed to the substrate phase speed, i.e. $v_m \approx v_s$, and the substrate speed is much greater than the layer phase speed, i.e. $v_m^2 >> v_l^2$, Eq. (41) can be reduced to,

$$\frac{\Delta v}{v_s} \approx \frac{-\rho_l \Delta d}{\rho_s w} \tag{43}$$

which is the result quoted by Martin *et al*[23]. However, it should be noted that the assumptions used to reduce Eq. (42) to Eq. (43) are very restrictive and may not apply in practice.

The perturbation results for the dependence on mass and frequency of the phase sensitivity of a bare substrate supporting shear waves to small mass loading depends on whether the substrate is operated as a Love wave device or a SH-APM device. Eq. (33) and Eq. (42) show that in the former case the dependence is $\Delta v/v_s \propto (\omega \Delta d)^2$ whilst in the latter case it is $\Delta v/v_m \propto \omega \Delta d$. In this section, perturbations about d=0 have been considered and the results are therefore only valid for the n=0 Love wave mode and associated APM modes. However, it is also possible to perform perturbations about the guiding layer thicknesses, d_{nm}, where the higher Love wave modes or their associated SH-APM's start; in effect the perturbations are about the mode speeds v_m.

V. Numerical Solutions and Discussion

To solve the dispersion equation (Eq. (14)) numerically the material parameters, (ρ_s, v_s, ρ_l, v_l) and the operating parameters (w, d, f) need to be specified. In general, for any given set of parameters there may be multiple solutions to the dispersion equation corresponding to multiple Love wave modes and multiple SH-APM's, so that the numerical approach needs to be relatively sophisticated. Defining the dimensionless layer thickness using the operating frequency $z=d/\lambda_l$ where $\lambda_l = v_l/f$, and the dimensionless combinations of the material parameters, $\mu_r = \mu_s/\mu_s$, $\beta=[1-(v_l/v_s)^2]^{1/2}$z and $w_r=w/d$, Eq. (14) can be re-written as,

$$\tan x = \mu_r \left(\frac{\beta}{x}\right) \sqrt{1-\left(\frac{x}{\beta}\right)^2} \tanh\left(\beta w_r \sqrt{1-\left(\frac{x}{\beta}\right)^2}\right) \tag{44}$$

In this equation, $x=T_l d$ is the variable which must be determined by the numerical routine. The mode phase speed, v, can then be found from x and the dimensionless form of Eq. (7),

$$\frac{v}{v_l} = \frac{1}{\sqrt{1-\left(\frac{x}{2\pi z}\right)^2}} \tag{45}$$

Once the mode speed has been determined, it can be used to compute the displacements in both the substrate and the layer. The solution of Eq. (43) can be considered for the two cases $(x/\beta)^2 \leq 1$ and $(x/\beta)^2 > 1$, which correspond to Love waves and SH-APM's, respectively. In both cases, the solution for x is real.

In the Love wave case, $(x/\beta)^2 \leq 1$ and the right-hand side of Eq. (44) is a monotonically reducing function of x which is infinite at $x=0$ and equal to zero at $x=\beta$. The left-hand side of Eq. (43) is a periodic function with infinities at $p\pi/2$ where $p=1, 3, 5, \ldots$ Hence, the number of solutions (Love wave modes) is determined by β and is 1+Int[β/π] where Int gives the integer part. In the Love wave case, increasing w_r reduces the value of x in the solution, so that for the same phase speed (Eq. (45)) z will be smaller. In the infinite thickness substrate case, the only dependence of the phase speed on d is in the combination $z=d/\lambda_l$ and this means that changing the guiding layer thickness is equivalent to changing λ_l. Since the wavelength is set by the operating frequency, f, this means that for Love waves on an infinite thickness substrate a change in guiding layer thickness is equivalent to a change in inverse frequency. For the finite thickness substrate case, this is no longer true because the length scale set by the operating frequency can be compared against w as well as d. In the SH-APM case, $(x/\beta)^2 > 1$ and the tanh( ) on the RHS of Eq. (44) becomes a tan( ) term, thus giving,

$$\tan x = -\mu_r \left(\frac{\beta}{x}\right)\sqrt{\left(\frac{x}{\beta}\right)^2 - 1}\,\tan\left(\beta w_r \sqrt{\left(\frac{x}{\beta}\right)^2 - 1}\right) \tag{46}$$

A further limitation, which is imposed by Eq. (45), is that $x<2\pi z$. When the substrate thickness is infinite ($w_r \to \infty$), no solutions exist to Eq. (45) satisfying $x>\beta$.

In the computation of the dispersion curve, Eq. (44) is solved by using fixed values of the substrate thickness w, the material parameters (ρ_s, v_s, ρ_l, v_l) and the operating frequency and starting with $d=0$. For the system without a guiding layer, the phase speeds for each mode, Love wave and SH-APM, are known from Eq. (23). The guiding layer thickness, d, is then increased incrementally and at each step Eq. (44) is solved iteratively for each mode using the previous solutions as the initial starting guesses; solutions to Eq. (44) include solutions to Eq. (46) and so it is only necessary to solve Eq. (44). Figure 2

shows a calculation using an operating frequency of 100 MHz with a polymer on quartz system described by material parameters ρ_s=2655 kg m^{-3}, v_s=5100 m s^{-1}, ρ_l=1000 kg m^{-3} and v_l=1100 m s^{-1}, and a substrate thickness of 100 μm. The operating frequency and the material parameters have been chosen because the system of PMMA on quartz using a surface skimming bulk wave (SSBW) has been widely reported in the literature on Love wave biosensors[24]. However, the substrate thickness is thinner than that typically used in Love wave biosensors and has been chosen to emphasise the SH-APM modes; the separation between SH-APM modes depends upon w. The number of modes possible when d=0 is given by $m_{\max}$=Int[$w\omega/\pi v_s$]=3. The initial speed of the Love waves and the associated SH-APM's and the thicknesses at which each of these modes begin is given in table I for the first three Love waves (n=0, 1, 2). These data points are shown in Fig. 2 as solid circles. The calculated phase speeds initially decrease slowly as the guiding layer thickness increases from zero, but in this system a sharp transition in speed occurs at approximately $d\sim\lambda_l/4$.

The existence of multiple modes and the possible change from real to imaginary of some functions as the mode speed converts from above v_s to below v_s, means that particular care is needed when evaluating the displacements (Eqs. (15) and (16) or (19)) associated with a particular solution of the dispersion equation (Eq. (14)). In order to group the terms in the displacements into factors that involve real functions multiplying travelling waves in the x_1 direction and either exponential decays or exponentials with phase factors, the displacements are re-written as

$$\underline{u}_l = (0,1,0)Af_l(x_3)\exp(-T_s w)e^{j(\omega t - k_1 x_1)} \tag{47}$$

and

$$\underline{u}_s = (0,1,0)Af_s(x_3)\exp(-T_s w)e^{j(\omega t - k_1 x_1)} \tag{48}$$

where the functions $f_l(x_3)$ and $f_s(x_3)$ are defined as,

$$f_l = \cosh(T_s w)\left[\cos(T_l x_3) + \tan(T_l d)\sin(T_l x_3)\right] \tag{49}$$

and

$$f_s = \cosh\left[T_s(x_3 + w)\right] \tag{50}$$

In the case of Love waves, T_s is real and positive, so that the displacement in the substrate and layer are given by the $f_s(x_3)$ and $f_l(x_3)$ functions each multiplied by the exp(-$T_s w$) function. In the case of SH-APM's, which have T_s imaginary, the displacement in the substrate and layer are given by the functions $f_s(x_3)$ and $f_l(x_3)$ alone. These two functions remain real, whereas the exp(-$T_s w$) factor becomes exp(-$jk_s w$) with k_s is real and so adds an overall phase factor into the travelling wave part of displacement.

Figure 3 shows the evolution of normalized displacements for the first Love wave (n=0 with m=0) as the guiding layer increases in thickness; the order of increasing guiding layer thickness is given by the sequence of solid curve, long dashes and short dashes. The layer displacement, $f_l\,(x_3)\exp(-T_s w)$ is shown for $x_3>0$ and the substrate displacement, $f_s\,(x_3)\exp(-T_s w)$, is shown for $x_3<0$ although only a small range of substrate depth is plotted; the displacements have been normalized so that they are unity at the top (free) surface of the guiding layer. The guiding layer thicknesses are given by d/λ_l=0.009726, 0.168272 and 0.363739 and correspond to phase speeds of 5099, 5050 and 1500 ms^{-1}, respectively; other parameters are the same as in Fig. 2. The guiding layer thicknesses have been chosen so that the evolution of the displacement for the first Love wave mode can be followed through the sharp transition in the phase speed shown in Fig. 2. Each of the displacements has an antinode at the top surface of the guiding layer and satisfy vanishing shear stress at the lower surface of the substrate; for an infinite thickness substrate this zero stress condition also implies a vanishing displacement. Initially, with a thin guiding layer, the substrate shows a displacement which has a shallow decay with depth and which is a good approximation to a constant in both the substrate and guiding layer. As the guiding layer thickness increases, a quarter wavelength type pattern in the layer becomes more dominant and the substrate displacement becomes relatively smaller and more like an exponential decay than a plane wave. Further increases in guiding layer thickness do not alter the basic quarter-wavelength pattern as the Love wave is already essentially localised in the layer. Physically, this is what we would expect. When the phase speed is close to that of the substrate, the Love wave has dominantly the properties of the shear wave in the substrate, e.g. a plane wave with $v\sim v_s$. However, when the phase speed is close to that of the guiding layer, the Love wave has dominantly the properties of the shear wave in the layer, e.g. localised in the layer with $v\sim v_l$ and having a node at the interface with the substrate so that it satisfies a quarter wavelength standing wave condition of $\lambda/4=d$ with $\lambda\sim\lambda_l$.

Figures 4 and 5 show the evolution of the second and third Love wave modes (n=1, m=0 and n=2, m=0) as the guiding layer thickness increases. The format of the figures is similar to Fig. 3 with increasing layer thickness in the sequence of solid curve, short dashes and long dashes. The second Love wave mode, shown in Fig. 4, begins its existence as a half wavelength pattern in the guiding layer. As the guiding layer thickness increases it evolves steadily into a $3\lambda/4=d$ pattern in the guiding layer, with $\lambda\sim\lambda_l$. Further increases in guiding layer thickness do not appreciably alter this pattern although the approximation $\lambda\approx\lambda_l$ becomes increasingly accurate. The evolution of the third Love wave mode, shown in Fig. 5, is similar to the previous cases. The pattern initially describes a full wavelength in the substrate, but as the speed drops and approaches the layer shear speed, the pattern evolves into a $5\lambda/4=d$ pattern in the guiding layer, with

$\lambda \sim \lambda_l$. Thus, the Love wave modes, labelled by n, each involve an initial pattern of $n\lambda/2=d$ in the guiding layer which then evolves into a $(2n+1)\lambda/4=d$ with $\lambda \sim \lambda_l$. This change in pattern matches the change in the Love wave mode speed from $v=v_s$ to $v \sim v_l$. These changes correspond to a change in Love wave character from that of a shear wave in the substrate to one that is similar to a shear wave in the guiding layer.

Figures 3-5 show how Love waves on a finite thickness substrate evolve in character as a solid guiding layer increases in thickness. Figure 6 shows the equivalent evolution for the SH-APM displacements, f_l (x_3) and f_s (x_3)., for the modes m=1, 2 and 3 associated with the n=0 Love wave. The displacements have been normalized to give unity at the top (free) surface of the guiding layer and the $\exp(-T_s w)$ functions are now phase factors and so combined into the travelling wave part of the displacements. In Fig. 6, each row corresponds to one SH-APM mode and the first diagram in the row shows the displacements as a function of relative depth into the substrate, x_3/w. The second diagram in the row shows the displacement as a function of the relative depth into the guiding layer, x_3/d and only a portion of the substrate is indicated so that the displacement in the guiding layer is emphasised. The evolution of the pattern for the first SH-APM (m=1, n=0 shown by Fig. 6 (a) and Fig. 6 (d)) takes a half wavelength in the substrate to a constant (plane wave) in the substrate. At the same time, the layer displacement evolves from a constant to a half wavelength type pattern. The guiding layer thicknesses are given by d/λ_l=0.001632, 0.218477 and 0.491484 and correspond to phase speeds of 5274, 5170 and 5102 ms^{-1}, respectively; other parameters are the same as in Fig. 2. The evolution of the next higher order SH-APM (m=2, n=0 shown by Fig. 6 (b) and Fig. 6 (e)) with increasing guiding layer thickness takes the substrate pattern from a wavelength to a half wavelength and the layer pattern from a constant to a half wavelength type. The guiding layer thicknesses are given by d/λ_l=0.003213, 0.242625 and 0.508397 and correspond to phase speeds of 5928, 5600 and 5275 ms^{-1}, respectively; other parameters are the same as in Fig. 2. The evolution of the subsequent higher order SH-APM (m=3, n=0 shown by Fig. 6 (c) and Fig. 6 (f)) with increasing guiding layer thickness takes the substrate pattern from a one and half wavelength to a wavelength and the layer pattern from a constant to a half wavelength. The guiding layer thicknesses are given by d/λ_l=0.0011375, 0.240673 and 0.505806 and correspond to phase speeds of 7918, 7000 and 5930 ms^{-1}, respectively; other parameters are the same as in Fig. 2. Thus, it is possible to visualise the evolution of any SH-APM associated with the n=0 Love wave with increasing guiding layer thickness. The m^{th} SH-APM associated with the n=0 Love wave starts with an $m\lambda/2$ type pattern in the substrate and a constant (plane wave) in the guiding layer. As the substrate thickness increases the pattern evolves until an $(m-1)\lambda/2$ type pattern is established in the substrate and a half wavelength type pattern is established in the substrate.

The physical interpretation arising from Fig. 6 can be extended to understand how any particular SH-APM mode associated with any particular Love wave mode evolves with increasing guiding layer thickness. The SH-APM mode, labelled by n and m, will initially have an $m\lambda/2$ type pattern in the substrate and an $n\lambda/2$ type pattern in the guiding layer. As the substrate thickness increases the patterns will evolve into an $(m\text{-}1)\lambda/2$ type pattern in the substrate and an $(n+1)\lambda/2$ type pattern in the guiding layer. This new pattern in the substrate and the layer then forms the starting point for the SH-APM mode associated with the next higher order $(n+1)$ mode Love wave. Once the SH-APM mode evolves into a plane wave pattern in the substrate it forms the basis for the "pure" Love wave mode with $m=0$. This latter interpretation can be seen from comparing the Fig. 6 (d) with Fig. 4. From comparison of Figs. 3-5 and Fig. 6, it is also possible to understand the sharp changes in phase speeds that occur as the guiding layer thickness increases as a mode transition. The transition of the m^{th} SH-APM to the $(m\text{-}1)^{th}$ SH-APM occurs from exactly the same guiding effect of the layer as the transition of the Love wave mode that leads to its phase speed changing from $v=v_s$ to $v\approx v_l$. The spectrum of initial phase speeds should be regarded as the sequence v_l, v_s, v_1, v_2, ….., $v_{\max}$ with increasing guiding layer thickness causing a transition between the successive phase speeds. This set of changes in the phase speeds can be seen clearly in Fig. 2, which shows that lowest order SH-APM mode eventually evolves into a higher order Love wave. In addition, each higher order SH-APM mode associated with one Love wave mode, evolves into the next lower order SH-APM mode associated with the next higher order Love wave mode.

The interpretation of SH-APM modes and their relationship to Love waves developed in this work may have significant consequences for the use of SH-APM's as sensors. The phase sensitivity of Love wave devices to deposited mass is high precisely because of the sharp change in the phase speed that can occur in the dispersion curve. A Love wave sensor is not operated with a thin guiding mass layer such that any additional mass being sensed can be regarded as a perturbation about $v=v_s$ (i.e. essentially $d=0$). Instead, the guiding layer thickness is selected to be at the steepest point on the phase speed-guiding layer thickness curve (i.e. at approximately $d\sim\lambda_l/4$). Any additional deposited mass then causes large changes in phase speed. In contrast, SH-APM sensors are generally operated without any guiding layer and mass being sensed is then a perturbation about the initial mode speed $v=v_m$ (i.e. $d=0$). The belief that Love wave devices are more sensitive sensors than SH-APM's, is therefore based on a comparison of perturbations of the SH-APM about the $d=0$ point of the dispersion curve and the Love wave about a $d\neq0$ point of the dispersion curve. A more valid comparison of sensitivity would be to use an SH-APM device that possessed a guiding layer of thickness producing the maximum slope in the dispersion curve (i.e. approximately $d\sim\lambda_l/4$). In this case, we would expect the sensitivity of the SH-APM to increase significantly. Moreover, the Love wave sensitivity arises from a transition in the phase speed from v_s to v_l

whereas with the layer guided SH-APM the transition will be between two mode speeds v_m and v_{m-1}. Since the SH-APM mode speeds are determined by substrate thickness, w, it should be possible to make the difference between the two highest modes greater than the difference between the substrate and layer speeds. Thus, with appropriately chosen parameters, the mass sensitivity of the layer guided SH-APM may even exceed that of the Love wave device; this we will describe fully in a future report.

VI. Conclusion

The propagation of shear horizontally polarized acoustic waves in a system of a finite substrate covered by a finite mass guiding layer of lower shear acoustic speed has been considered. A dispersion equation and the solutions for the substrate and layer displacements have been constructed. The structure of the equations has been examined and multiple solutions predicted. These solutions have been shown to be analogous to Love waves when $v \leq v_s$ and to SH-APM's when $v > v_s$. This formulation includes the generalisation of Love waves to Love waves on finite substrates and the generalisation of SH-APM's to layer guided SH-APM's; together we refer to these modes as generalised Love waves. Perturbation theory has been used to derive the fractional shift in phase speed produced by small mass (thin guiding) layers. It has been argued that the perturbed $m=0$ SH-APM, referred to in the literature, does not exist, but is in fact a perturbed Love wave. Numerical solutions to the dispersion equation have been constructed and the displacements in the substrate and guiding layer examined. These show that the higher order Love wave modes evolve out of the lower order SH-APM's and the SH-APM's associated with one Love wave arise from the SH-APM's from the next lower order Love wave. It has been suggested from the new interpretation of SH-APM's and the development of a theory for layer guided SH-APM's, that sensors with significantly higher mass sensitivity will be possible.

Acknowledgements

The authors' gratefully acknowledge the BBSRC for financial support under research grant 301/E11140. We would also like to acknowledge Dr E. Gizeli and Dr K. A. Melzak for discussions on the topic of Love waves.

References

[1]H. Wohltjen and R. Dessy, Anal. Chem. **51**, 1458 (1979).

[2]A. A. Oliner, *Acoustic surface waves* (Springer-Verlag, Berlin, 1978).

[3]R. M. White, Faraday Discuss. **107**, 1 (1997).

[4]G. Z. Sauerbrey, Z. Phys. **155**, 206 (1959).

[5]K. K. Kanazawa and J. G. Gordon, Anal. Chim. Acta. **175**, 99 (1985).

[6]S. Bruckenstein and M. Shay, Electroch. Acta. **30**, 1295 (1985).

[7]E. M. Pater, S. Bruckenstein and A. R. Hillman, J. Chem. Soc., Fraday Trans. **94**, 1097 (1998).

[8]B. A. Cavic, G. L. Hayward and M. Thompson, Analyst **124**, 1405 (1999).

[9]S. Rösler, R. Lücklum, R. Borngraber, J. Hartmann and P. Hauptmann, Sens. Actuators B **48**, 415 (1998).

[10]G. McHale, M. K. Banerjee, M. I. Newton and V. V. Krylov, Phys. Rev. B **59**, 8262, (1999).

[11]R. W. Cernosek, S. J. Martin, A. R. Hillman and H. L. Bandey, IEEE Trans. Ultrason. Ferroelectr. Freq. Control **45**, 1399 (1998).

[12]G. McHale, R. Lücklum, M. I. Newton and J. A. Cowen, J. Appl. Phys. **88**, 7304 (2000).

[13]R. M. White and F. Voltmer, Appl. Phys. Lett. **7**, 314 (1965).

[14]B. A. Auld, J. J. Gagnepain and M. Tan, Electron. Lett. **12**, 650 (1976).

[15]H. Engan, KI. A. Ingebrigtsen and A. Tonning, Appl. Phys. Lett. **10**, 311 (1967).

[16]T. I. Browning and M. F. Lewis, *Electron. Lett.* **13**, 128 (1977).

[17]A. E. H. Love, *Some problems of Geodynamics* (Cambridge Univ. Press, Cambridge, 1911; New York Dover, 1967).

[18]D. P. Morgan, *Surface-wave devices for signal processing* (Elsevier, New York, 1991).

[19]E. Gizeli , A. C. Stevenson, N. J. Goddard and C. R. Lowe , IEEE Trans. Ultrason. Ferroelec. Freq. Control. **39**,657 (1992).

[20]M. F. Lewis, Electron. Lett. **17**, 819 (1981).

[21]A. J. Ricco and S. J. Martin, Appl. Phys. Lett. **50**, 1474 (1987).

[22]D. S. Ballantine, R. M. White, S. J. Martin, A. J. Ricco, E. T. Zellers, G. C. Frye and H. Wohltjen, *Acoustic wave sensors* (Academic Press, New York, 1997).

[23]S. J. Martin, A. J. Ricco, T. M. Niemczyk and G. C. Frye, Sens. Act. **20**, 253 (1989).

[24]E. Gizeli, Anal. Chem. **72**, 5967 (2000).

Table I

Phase speed, v, and normalised layer thickness, d/λ_l, at which Love waves and SH-APM's begin for first three Love wave modes; parameters are ρ_s=2655 kg m^{-3}, v_s=5100 ms^{-1}, ρ_l=1000 kg m^{-3}, v_l=1100 m s^{-1}, w=100 μm and f=100 MHz.

v/ ms^{-1}	d_{0m}/λ_l	d_{1m}/λ_l	d_{2m}/λ_l
5100.00	0.0	0.512052	1.02410
5274.36	0.0	0.511242	1.02248
5929.03	0.0	0.508834	1.01767
7918.88	0.0	0.504895	1.00979

Figures

Figure 1. Definition of axes and propagation direction for shear horizontally polarized waves in a system of a finite substrate covered by a finite mass guiding layer; the displacement is in the x_2 direction.

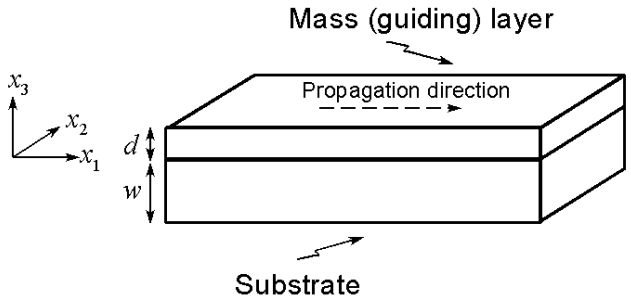

Figure 2 Theoretical calculated phase speeds (solid curves) as a function of normalised guiding layer thickness ($d/\lambda_l = df/v_l$) showing multiple modes of Love waves ($v<v_s$) and the associated acoustic plate modes ($v>v_s$). The solid circle symbols indicate the analytical result for the start of each mode.

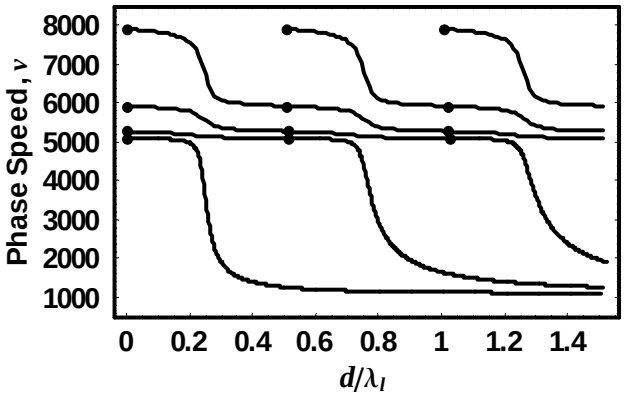

Figure 3 Evolution of the displacements of the guiding layer and substrate for the first Love wave (n=0 and m=0) as the layer thickness increases (solid, long dash, short dash); the surface normal co-ordinate, x_3, has been normalised by the layer thickness. Layer and substrate parameters are the same as in Fig. 2.

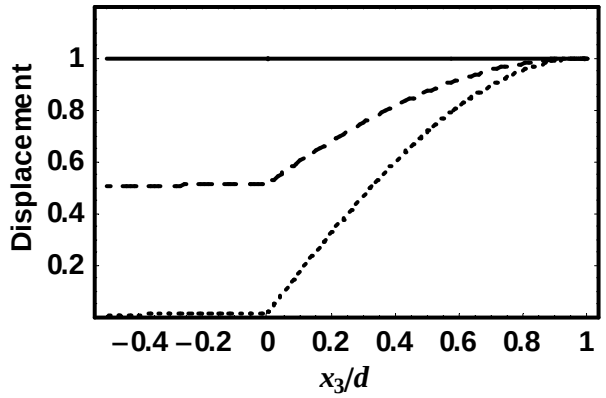

Figure 4 Evolution of the displacements of the guiding layer and substrate for the second Love wave (n=1 and m=0) as the layer thickness increases (solid, long dash, short dash); the surface normal co-ordinate, x_3, has been normalised by the layer thickness. Layer and substrate parameters are the same as in Fig. 2.

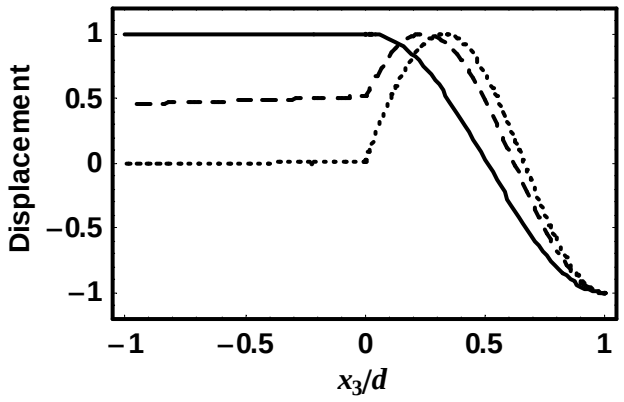

Figure 5 Evolution of the displacements of the guiding layer and substrate for the third Love wave (n=2 and m=0) as the layer thickness increases (solid, long dash, short dash); the surface normal co-ordinate, x_3, has been normalised by the layer thickness. Layer and substrate parameters are the same as in Fig. 2.

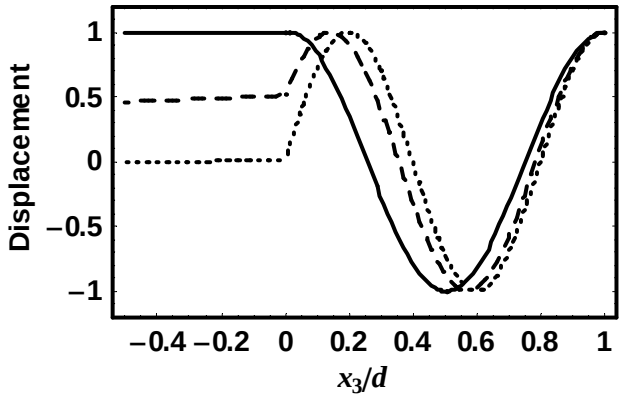

Figure 6. Evolution of the displacements of the substrate and guiding layer for the first three layer guided SH-APM's associated with the first Love wave as the layer thickness increases (solid, long dash, short dash). Diagrams (a) to (c) show the displacement as a function of the surface normal co-ordinate, x_3, normalised by the substrate thickness, w, for modes m=1, 2 and 3 respectively each with n=0. Diagrams (d) to (f) correspond to the same displacements, but as a function of the surface normal co-ordinate, x_3, normalised by the guiding layer thickness, d.